bioRxiv preprint doi: https://doi.org/10.1101/446732; this version posted October 18, 2018. The copyright holder for this preprint (which was not certified by peer review) is the author/funder, who has granted bioRxiv a license to display the preprint in perpetuity. It is made available under aCC-BY-NC 4.0 International license.

Conformational states control Lck switching between free and confined diffusion modes in T cells

Geva Hilzenrat[1, 2], Elvis Pandžić[3], Zhengmin Yang[1, 2], Daniel J. Nieves[1, 2], Jesse Goyette[1,2], Jérémie Rossy[4], Katharina Gaus[1, 2]*

[1]*EMBL Australia Node in Single Molecule Science, School of Medical Sciences, University of New South Wales, Sydney, Australia*

[2]*ARC Centre of Excellence in Advanced Molecular Imaging, University of New South Wales, Sydney, Australia*

[3]*BioMedical Imaging Facility, Mark Wainwright Analytical Centre, University of New South Wales, Sydney, Australia*

[4]*Biotechnology Institute Thurgau, University of Konstanz, Kreuzlingen, Switzerland*

*Corresponding author: k.gaus@unsw.edu.au

Abstract

T cell receptor (TCR) phosphorylation by Lck is an essential step in T cell activation. It is known the conformational states of Lck control enzymatic activity; however, the underlying principles of how Lck finds its substrate in the plasma membrane remain elusive. Here, single-particle tracking is paired with photoactivatable localization microscopy (sptPALM) to observe the diffusive modes of Lck in the plasma membrane. Individual Lck molecules switched between free and confined diffusion in resting and stimulated T cells. Conformational state, but not partitioning into membrane domains, caused Lck confinement as open conformation Lck was more confined than closed. Further confinement of kinase-dead versions of Lck suggests that Lck interacts with open active Lck to cause confinement, irrespectively of kinase activity. Our data supports a model that confined diffusion of open Lck results in high local phosphorylation rates and closed Lck diffuses freely to enable wide-range scanning of the plasma membrane.

bioRxiv preprint doi: https://doi.org/10.1101/446732; this version posted October 18, 2018. The copyright holder for this preprint (which was not certified by peer review) is the author/funder, who has granted bioRxiv a license to display the preprint in perpetuity. It is made available under aCC-BY-NC 4.0 International license.

T cell signaling is a tightly controlled process involving both simultaneous and sequential spatiotemporal events, involving membrane remodeling and redistribution of key signaling proteins [1,2]. Engagement of the T cell receptor (TCR) with an antigenic pMHC on the surface of an antigen-presenting cell (APC) leads to the formation of immunological synapses [3] and initiates downstream signaling events that lead to T cell activation [4]. The Src family kinase Lck plays a crucial role in the signaling cascade. TCR engagement results in the membrane release [5] and phosphorylation of the immunoreceptor tyrosine-based motifs (ITAMs) located in the cytoplasmic tails of the CD3ζ chain by Lck [6]. Phosphorylated sites on the TCR-CD3 complex become docking sites for the zeta chain-associated protein kinase 70 (ZAP70), that is further phosphorylated by Lck [7] before recruiting other proteins in the signaling cascade that are necessary for complete T cell activation.

The role of Lck in T cell activation as a signaling regulator is of particular interest due to its dynamic characteristics. Lck is a 56 kDa protein comprised of a Src homology (SH) 4 domain at the N-terminus, followed by a unique domain, an SH3 domain, an SH2 domain, a kinase domain and short C-terminal tail. Lck is anchored to the plasma membrane through its SH4 domain via post-translational acylation on three specific sites: a myristoylated Gly2 [8] and palmitoylated Cys3 and Cys5. The latter two are crucial for membrane binding and biological activity, enabling Lck diffusion in the inner leaflet of the plasma membrane and its recruitment to the immunological synapse [9]. The unique domain interacts with the CD3ε subunit in the TCR-CD3 complex [10] as well as the co-receptors CD4 and CD8 [11] via zinc-mediated bonds. However, Lck does not require the co-receptors for recruitment to the immunological synapse or for TCR triggering [12], suggesting that freely diffusing Lck is sufficient for T cell activation.

Lck conformation is regulated by the phosphorylation of two tyrosine residues: Tyr^{394}, where phosphorylation increases Lck activity, and Tyr^{505}, whose phosphorylation reduces Lck

bioRxiv preprint doi: https://doi.org/10.1101/446732; this version posted October 18, 2018. The copyright holder for this preprint (which was not certified by peer review) is the author/funder, who has granted bioRxiv a license to display the preprint in perpetuity. It is made available under aCC-BY-NC 4.0 International license.

activity [13,14]. Intramolecular interactions between the phosphorylated Tyr^{505} ($pTyr^{505}$) and the SH3 and SH2 domains cause rearrangements that keep Lck in a closed, inactive conformation [15,16]. When dephosphorylated by CD45, Lck exists in an open, primed conformation. When Tyr^{394} is trans-autophosphorylated [14], rearrangements in the activation loop stabilize the active conformation [17]. Lck's diffusion behavior [18] and conformational state [19,20] are thought to be regulated by the activation state of the cell. The conformational state also influences Lck clustering [21]. This means that not only does Lck conformational state regulate Lck enzymatic activity but also aids in its diffusive search strategy.

Whether Lck becomes 'active', i.e., converted into the open conformation upon TCR engagement, has been controversial. There is evidence of global changes in relative populations of closed and open Lck in resting *versus* stimulated T cells [19,20]. These studies propose that Lck undergoes conformational changes upon T cell activation, driving it from its closed state to an open state, therefore enhancing its activity. Using biochemical analyses, conformational heterogeneity was observed in resting and stimulated T cells [22], suggesting a "standby-model" in which ~40% of Lck is in the open conformation in both resting and stimulated T cells. Ballek et al. challenged these observations in a later report that used different cell lysis conditions [23]. Another study, based on measurements of fluorescence resonance energy transfer (FRET) between fluorescent proteins fused to the N- and C-terminals of Lck, concluded there was no significant change in open *versus* closed populations of Lck even after T cell stimulation [24]. While different papers report different percentages of open Lck in pre-stimulated cells, constitutively active Lck were also found in $CD8^+$ memory T cells and may account for the enhanced sensitivity to antigen in these cells [25]. A pool of active Lck existing prior to T cell stimulation led to the idea that rapid TCR triggering post receptor engagement may be caused by changes in Lck spatial rearrangements as opposed to, or in addition to conformational changes. Using single-molecule localization

bioRxiv preprint doi: https://doi.org/10.1101/446732; this version posted October 18, 2018. The copyright holder for this preprint (which was not certified by peer review) is the author/funder, who has granted bioRxiv a license to display the preprint in perpetuity. It is made available under aCC-BY-NC 4.0 International license.

microscopy in fixed cells, we previously showed that Lck distributed differently on the cell surface depending on its conformational state [21], with open Lck residing preferentially in clusters and closed Lck preventing clustering, regardless of the cell's activation state. However, this study only captured the overall distribution of open or closed Lck and the movement of Lck clusters, but to understand the search strategy of the membrane-bound kinase the dynamic behavior of individual molecules need to be taken into account.

The efficiency of a dual-state search strategies has previously been demonstrated in other systems [26]. For Lck, such a strategies would entail that individual molecules oscillate between two distinct states: a confined state that corresponds to high Lck activity and a diffusive state that enables the kinase to scan the membrane for substrates. Such a dual-state search strategy may account for the high fidelity of Lck-mediated phosphorylation of the available TCR-CD3 complexes while also retaining high signaling sensitivity when membrane-detached cytosolic tails of the CD3 complex are limited. The former would be mediated by the high enzymatic activity in Lck clusters while the high level of diffusion of Lck in the closed state would enable the latter.

The dynamic behavior of Lck was previously mapped with single particle tracking (SPT) in live cells, revealing, for example, the differences in Lck diffusion in stimulated *versus* resting T cells and the formation of microclusters, but without linking dynamics to conformational states [18,27]. Overall changes in diffusion constants were observed, as well as segregation into different confinement zones, attributed to actin and other proteins compartmentalizing the membrane [27,28] or to the formation of membrane microdomains [18]. Recently, Lck compartmentalization upon TCR stimulation was attributed to the formation of close-contact zones between the T cell membrane and the stimulating surface, possibly because of exclusion of CD45, in line with the kinetic segregation model [29]. These works, however, did not take into account the conformational change in Lck.

bioRxiv preprint doi: https://doi.org/10.1101/446732; this version posted October 18, 2018. The copyright holder for this preprint (which was not certified by peer review) is the author/funder, who has granted bioRxiv a license to display the preprint in perpetuity. It is made available under aCC-BY-NC 4.0 International license.

105 In the current study, we utilize SPT using photoactivatable localization microscopy
106 (sptPALM) [30] as a tool to study the diffusion of wild type (WT) and mutated Lck, lacking the
107 tyrosine residues on positions 394 and 505, to measure the dynamics of the closed and open
108 forms, respectively [19,20]. Lck variants were tagged with photoactivatable monomeric cherry
109 (PAmCherry) [31], expressed in Jurkats 1.6E cells and imaged in resting and activating
110 conditions. Single trajectories were extracted and analyzed in order to find periods when the
111 proteins underwent confined diffusion and the fraction of confined versus free proteins was
112 determined [32]. Measurements of different Lck variants showed that conformation has a key
113 role in Lck's substrate search strategy, with the open form dwelling more in confinements
114 compared to the closed form. Further, we provide evidence of Lck-Lck interaction in the
115 open conformation in stimulated T cells. Taken together, the data suggest that Lck
116 continuously switched between open and closed states, which is likely to determine the
117 probability of productive encounters between Lck and its substrates.

118 # Results

119 ## Identification of free and confined states of Lck in live T cells

120 In order to characterize the diffusion patterns of Lck, we applied single particle tracking on
121 image sequences from different experimental conditions and decomposed each trajectory into
122 free and confined segments. Jurkat E6.1 cells were transfected with either wild-type Lck
123 (wtLck) fused to PAmCherry (wtLck-PAmCherry) or a truncated construct of Lck containing
124 only the first ten amino acids that are responsible for Lck anchoring to the membrane (Lck10-
125 PAmCherry). T cells were stimulated for ~5 minutes at 37°C on a coverslip coated with anti-
126 CD3 and anti-CD28 antibodies and imaged either in live-cell conditions or after chemical
127 fixation. In each experiment we acquired 10,000 frames with an 18 ms exposure for the
128 duration of ~197 s. Imaging was done while continuously photo-activating and exciting the

bioRxiv preprint doi: https://doi.org/10.1101/446732; this version posted October 18, 2018. The copyright holder for this preprint (which was not certified by peer review) is the author/funder, who has granted bioRxiv a license to display the preprint in perpetuity. It is made available under aCC-BY-NC 4.0 International license.

fluorophores. Trajectories shorter than 15 frames and immobile particles (particles with a low RMSD, as described in the Methods section) were excluded from analysis.

We decomposed trajectories by adopting a previously described post-tracking analysis [32]. Briefly, every trajectory is first fragmented into overlapping windows. For each window, the normalized variance of the location of the particle is calculated as a measure of the level of confinement, L_{Conf}, according to:

$$(1)\quad L_{Conf} = \frac{D_{free} \times W \times t_W}{var(r)}$$

where D_{free} is the diffusion coefficient of freely diffusing Lck in $\mu m^2\ sec^{-1}$, W is the window size in frames, t_W is the temporal length of the window in seconds and var(r) is the variance in μm^2. We chose the diffusion coefficient of Lck10-PAmCherry as the value for D_{free} for all versions of Lck as Lck10 is membrane anchored but does not interact with other proteins. We then defined a threshold of L_{Conf} above which particles are considered confined. For this threshold, we chose the most abundant L_{Conf} value for wtLck-PAmCherry in stimulated T cells, following the procedure published previously [32] (dotted line in Fig. 1A). This threshold was suitable because the majority of values for Lck10-PAmCherry in resting cells were below this threshold and all values for wtLck-PAmCherry in fixed cells were above the threshold (Fig. 1A). In order to ensure that Lck molecules were in fact confined, rather than just temporarily slowing down, we only regarded a molecule as confined if it has an L_{Conf} value above the threshold for three or more consecutive windows. Trajectories were then segmented into confined and free periods (Fig. 1B), depending on whether L_{Conf} was above or below the threshold (Fig. 1C). From this analysis it was evident that molecules that diffused slowly for 3 or more consecutive states were found to be confined (Fig. S1). This analysis was applied to all trajectories recorded in a cell (Fig. 1D). As is evident from this sptPALM analysis, individual wtLck-PAmCherry molecules in live cells switched between free and

bioRxiv preprint doi: https://doi.org/10.1101/446732; this version posted October 18, 2018. The copyright holder for this preprint (which was not certified by peer review) is the author/funder, who has granted bioRxiv a license to display the preprint in perpetuity. It is made available under aCC-BY-NC 4.0 International license.

confined diffusive states (Fig. 1D) while in fixed cells, only confined or immobile molecules were observed (Fig. 1D).

Wild-type Lck was more confined in stimulated than resting T cells

Previous studies provided evidence that T cell activation decreases the overall diffusion of Lck [18,27]. In our experiments, resting T cell data was generated by placing T cells expressing wtLck-PAmCherry onto coverslips coated with anti-CD90 antibodies. This resulted in good T cell adhesion, but not TCR signaling or T cell activation [33]. Our measurements confirmed the decrease in diffusion (Fig 2A; Movie S1: resting - right, stimulated - left), with diffusion coefficients of 1.16 $\mu m^2\ s^{-1}$ (1.15-1.17) to 0.69 $\mu m^2\ s^{-1}$ (0.68-0.7) for resting and stimulated cells, respectively (Fig. 2A, Fig. S2a; Movie S1). We wanted to assess whether this slowdown is caused by enhanced spatial compartmentalization in the membrane. Thus, we conducted the L_{Conf} analysis for wtLck-PAmCherry in resting and stimulated cells. When comparing the L_{Conf} histogram of wtLck in stimulated T cells (Fig. 2B, blue) *versus* resting T cells (Fig. 2B, orange), it is noticeable that the values in activated cells are shifted to higher values, resulting in a mean L_{Conf} value of 32.9 in stimulated cells and 29.1 in resting cells.

Next we examined whether the decrease in local displacement variance is due to a redistribution of wtLck-PAmCherry into confinements that would result in an increase in the number of consecutive steps that fall above the L_{Conf} threshold value. Thus, we segmented the total video into segments of five frames (Fig. S3), in which we asked how many particles, out of the total number of particles imaged, were confined. Histograms obtained for stimulated and non-stimulated cells (Fig. 2C) were collected. There was a clear difference in peak value for the two populations as well as a larger tail of high values for wtLck-PAmCherry in stimulated cells. As a consequence, the populations were statistically different (Fig. 2C) when tested against the null hypothesis according to which the samples are drawn from the same

bioRxiv preprint doi: https://doi.org/10.1101/446732; this version posted October 18, 2018. The copyright holder for this preprint (which was not certified by peer review) is the author/funder, who has granted bioRxiv a license to display the preprint in perpetuity. It is made available under aCC-BY-NC 4.0 International license.

177 population, using the rank sum test, with different medians and non-overlapping 95%
178 confidence intervals with the values of 27.27% (26.67-27.78) and 22.22% (21.82-22.73) for
179 stimulated and resting cells, respectively. The percentage of confined wtLck-PAmCherry
180 were 30.97% (30.63-31.3) and 26.4% (26.14-26.68) in stimulated and resting cells,
181 respectively.

182 Overall, these results show that wtLck-PAmCherry diffused slower in stimulated cells
183 compared to resting cells, suggesting that in addition to a global reduction in diffusion, a
184 redistribution of Lck into confinements had occurred. These results are in agreement with an
185 increase in wtLck-PAmCherry clustering in fixed stimulated *versus* fixed resting T cells [21].

186 **Membrane anchoring alone is not contributing to Lck confinement**

187 Lck confinement may be attributed to the formation of membrane domains, i.e., changes in
188 membrane order , as a result of TCR triggering [34]. If that is the case, a truncated version of
189 Lck, Lck10, that includes the first ten amino acids that are responsible to Lck anchoring to
190 the membrane as it contains the post-translational lipid modifications, is expected to
191 experience the same slowdown and confinement as full-length Lck. However, we did not
192 observe such a scenario (Fig. 3A; Movie S2), as the diffusion coefficients found for Lck10-
193 PAmCherry in stimulating and resting conditions remained high (Fig. S2b). The overall level
194 of confinement of Lck10-PAmCherry was almost identical for both resting and stimulated
195 cells, with a peak L_{Conf} value of 7.2 and 7.74, respectively (Fig. 3B). These values were
196 significantly different from the ones found for wtLck-PAmCherry, with most of the
197 probability function having a value below the threshold described above. A histogram of
198 confinement events (Fig. 3C) shows comparable peak values for both stimulated and resting
199 cells. No statistically significant difference was found between the two samples (Fig. 3C, top
200 panel), as shown by median of 9.62% (9.43-9.8) and 9.68% (9.52-10.00) for Lck10-

bioRxiv preprint doi: https://doi.org/10.1101/446732; this version posted October 18, 2018. The copyright holder for this preprint (which was not certified by peer review) is the author/funder, who has granted bioRxiv a license to display the preprint in perpetuity. It is made available under aCC-BY-NC 4.0 International license.

PAmCherry expressed in stimulated and resting cells, respectively. Further, the mean fraction of confined particles was slightly higher in resting cells, with values of 13.96% (13.74-14.18) and 14.73% (14.45-15.00) for stimulated and resting cells, respectively. These values were lower than those found for wtLck-PAmCherry, suggesting Lck10-PAmCherry was far less confined than wtLck-PAmCherry, even in stimulated cells.

Taken together, the data strongly suggest that the increased confinement observed for full-length wtLck-PAmCherry was not due to global changes in membrane organization or membrane domains [18] as confinement of Lck10 in resting and stimulated T cells was similar.

Open Lck is highly confined in stimulated and resting cells

Previously, we reported that Lck clustering was regulated by the kinase's conformational state [21]. We thus quantified the influence of conformation on confinement of Lck in live cells. First, we introduced a Tyrosine-to-Phenylalanine mutation at position 505 in Lck (Lck^{Y505F}). The mutation prevents the binding of Lck $pTyr^{505}$ to its own SH2 domain. This mutation is well known as 'constitutively open' [19-21,24,35] and 'hyperactive' [13]. An overall change in the diffusion constants due to cell activation (Fig. 4A; Movie S3) was observed, with values of 0.65 $\mu m^2\ s^{-1}$ (0.64-0.66) and 0.95 $\mu m^2\ s^{-1}$ (0.94-0.96) in stimulated and resting cells, respectively (Fig. S2c). Further, L_{Conf} values for Lck^{Y505F}-PAmCherry were higher than that of wtLck-PAmCherry (Fig. 4B), with peak values of 39.28 and 42.53 in stimulated and resting cells, respectively, with <50% of $\log_{10}(L_{Conf})$ events above the confinement threshold. In contrast to wtLck-PAmCherry, the L_{Conf} distributions of Lck^{Y505}-PAmCherry were similar in resting and stimulated T cells. This similarity was also observed in the histograms of the confined fractions (Fig. 4C), with a large population of Lck^{Y505} molecules falling into the right tail of the distribution. Importantly, unlike in the corresponding data for wtLck-PAmCherry, these values were not significantly different from each other (Fig. 4C, top), with

bioRxiv preprint doi: https://doi.org/10.1101/446732; this version posted October 18, 2018. The copyright holder for this preprint (which was not certified by peer review) is the author/funder, who has granted bioRxiv a license to display the preprint in perpetuity. It is made available under aCC-BY-NC 4.0 International license.

median values and overlapping 95% confidence interval of 26.55% (26.32-26.67) and 26.39% (26.14-26.67) for stimulated and resting cells, respectively. The means of Lck^{Y505} were 29.85% (29.59-30.11) and 29.97% (29.74-30.22) in stimulated and resting cells, respectively.

These data show that when Lck is locked in the open state, it is also driven into a more confined diffusive behavior, which is comparable with wtLck-PAmCherry in stimulated cells (Fig. S4). Although the diffusion coefficient found for Lck^{Y505F}-PAmCherry is lower, in terms of confinement, open Lck was insensitive to the T cell activation with Lck^{Y505F}-PAmCherry confinement levels being similar in both stimulated and resting cells. This indicates that Lck confinement is driven by the open conformation of the kinase and supports that a higher proportion of Lck is in the open conformation in stimulated T cells [19,20,36].

Closed Lck is as confined as wild-type Lck in resting cells

To further investigate the hypothesis that Lck conformation regulates Lck diffusive behavior, we expressed a closed form of Lck in Jurkat cells. A mutation in position 394 converting a tyrosine into phenylalanine (Lck^{Y394F}) prevents the formation of the activation loop and results in reduced-activity [14] or an inactive Lck [13] because of the hyper-phosphorylated tyr^{505} [22] that constitutively closes the enzyme [19].

As with the wtLck and Lck^{Y505F}, Lck^{Y394F}-PAmCherry did undergo a decrease in diffusion coefficient due to stimulation (Fig.5A; Movie S4), from 1.24 $\mu m^2 s^{-1}$ (1.22-1.26) in resting cells to 0.88 $\mu m^2 s^{-1}$ (0.87-0.89) in stimulated cells (Fig. S2d). We applied the same sptPALM analysis to Lck^{Y394F}-PAmCherry and lower L_{Conf} values were obtained with peak values of 32.93 and 30.36 in stimulated and resting cells, respectively (Fig. 5B). Histograms of the fraction of confined Lck^{Y394F}-PAmCherry showed the populations were skewed towards lower values (Fig. 5C). Similarly to Lck^{Y505F}-PAmCherry, Lck^{Y394F}-PAmCherry

bioRxiv preprint doi: https://doi.org/10.1101/446732; this version posted October 18, 2018. The copyright holder for this preprint (which was not certified by peer review) is the author/funder, who has granted bioRxiv a license to display the preprint in perpetuity. It is made available under aCC-BY-NC 4.0 International license.

showed no statistically significant difference between stimulated and resting cells (Fig. 5C, top panel) and medians of 22.22% (21.88-22.58) and 21.95% (21.43-22.22) for Lck^{Y394F}-PAmCherry in stimulated and resting cells, respectively. The mean confinement fractions were 26.09% (25.85-26.33) and 26.24% (25.92-26.55) for Lck^{Y394F}-PAmCherry in stimulated and resting cells, respectively.

The confinement fraction values we found for the closed Lck were smaller than the ones found for the open Lck (Fig. S4), illustrating the significance conformational states have on Lck diffusion. Indeed closed Lck has a similar level of confinement as wtLck in resting cells while open Lck was similarly confined as wtLck in activated cells (Fig. S4). Thus, the data confirms that confinements are regulated by the conformational state of Lck with open Lck being more confined and closed Lck being less confined.

Lck self-associates with other Lcks, depending on its conformation and activity

An open Lck that is also phosphorylated in Tyrosine 394 is known to be active, while studies done on Lck^{Y505F} showed hyperactivity [13,14]. By expressing a constitutively inactive Lck, we could assess whether Lck confinement relies on enzymatic activity. We tested an Lck variant in which the lysine in position 273 in the kinase domain is replaced with Arginine (Lck^{K273R}-PAmCherry, Fig. 6, Fig. S5), which has been shown to render Lck kinase-dead [37]. Different diffusion coefficients of 0.82 $\mu m^2 s^{-1}$ (0.81-0.83) and 1.13 $\mu m^2 s^{-1}$ (1.12-1.15) were observed for Lck^{K273R}-PAmCherry in stimulated and resting cells, respectively (Fig. S2e). However, similar L_{Conf} histograms, with values of 34.80 for stimulated and 37.58 for resting cells, were obtained (Fig. 6B, blue and orange) with no significant difference observed in the fraction of time spent confined (Fig 6C, blue and orange). Additionally, Lck^{K273R}-PAmCherry spent 25.80% (25.56-26.07) and 25.62% (25.38-25.86) of time confined in stimulated and resting cells, respectively (Fig 6C). Thus, the level of confinement kinase-dead Lck did not depend

bioRxiv preprint doi: https://doi.org/10.1101/446732; this version posted October 18, 2018. The copyright holder for this preprint (which was not certified by peer review) is the author/funder, who has granted bioRxiv a license to display the preprint in perpetuity. It is made available under aCC-BY-NC 4.0 International license.

on the T cell activation status as it did for wtLck (Fig. S5). Assuming that the K273R mutation disables Lck activation via autophosphorylation, as hypothesized previously [13], the finding suggest that confinement of wtLck in stimulated T cells is regulated by Lck activation.

To further test this hypothesis, we expressed a constitutively-open kinase-dead mutant $Lck^{K273R,\ Y505F}$-PAmCherry. This mutant had slower diffusion coefficients of 0.41 $\mu m^2\ s^{-1}$ (0.41-0.42) and 0.51 $\mu m^2\ s^{-1}$ (0.5-0.51) in stimulated and resting cells, respectively (Fig. 6A; Fig. S2f; Movie S5), values that were slower than those obtained for Lck^{K273R}-PAmCherry (Fig. S2e, f). Further, $Lck^{K273R,\ Y505F}$-PAmCherry had higher L_{Conf} values in stimulated cells (Fig. 6C, purple and yellow) compared to resting cells (44.78 and 35.09, respectively).

Conducting the same analysis to quantify confinement fractions, we found a large fraction of kinase-dead mutant in the open conformation was highly confined in stimulated cells (Fig. 6C, purple and yellow). When comparing total trajectories, $Lck^{K273R,\ Y505F}$-PAmCherry in stimulated cells was more confined than in resting cells and more than Lck^{K273R} in both cell activation statuses (Fig. S5). These data confirm the conclusion that open, but not necessarily enzymatically active Lck confined the kinase in distinct zones in the plasma membrane.

$Lck^{K273R,\ Y505F}$-PAmCherry was more confined in stimulated cells (26.97% (26.76-27.18)) than resting cells (23.30% (23.08-23.52)). It is possible that the open, kinase-dead variant of Lck interacts with endogenous Lck in Jurkat cells that were already shown to be confined in stimulated cells (Fig. 2). This would suggest that open Lck is confined in activated T cells by Lck-Lck interaction. Moreover, the lowered confinement for the K273R-Y505F mutant in resting cells compared to stimulated cells excludes the possibility of confinement due to increase in hydrodynamic radius of the enzyme (Fig. S5). Taken together, the experiments with the kinase-dead version of Lck confirmed the finding that it was the open conformation

bioRxiv preprint doi: https://doi.org/10.1101/446732; this version posted October 18, 2018. The copyright holder for this preprint (which was not certified by peer review) is the author/funder, who has granted bioRxiv a license to display the preprint in perpetuity. It is made available under aCC-BY-NC 4.0 International license.

297 that caused the Lck confinement. Thus it is likely that the enzyme switches between open and
298 close conformation, which results in a dual-state search strategy where open and active Lck is
299 confined, and closed and inactive Lck diffuses freely (Fig. 7).

300

301 **Discussion**

302 Phosphorylation of the TCR-CD3 complex by the kinase Lck is an essential step in T cell
303 activation [38]. While it is relatively well documented that the conformational states control
304 enzymatic activity, how membrane-bound Lck finds and phosphorylates its substrates is not
305 well understood. For example, the link between phosphorylation state and activity is well
306 established [39], as well as some interactions of Lck with other proteins [40-43] and lipids [44]. Most
307 studies so far have focused on whether or not T cell stimulation results in an 'activation' of
308 Lck itself, i.e., whether there is an overall increase of Lck molecules in the open
309 conformation and whether a stable pool of open Lck already exists in resting T cells.
310 However, it is also possible that in the dynamic environment of the inner leaflet of the plasma
311 membrane, Lck switches between open and closed states, as many other types of enzymes do
312 [45-47]. Utilizing single molecule localization microscopy (SMLM) techniques, our group
313 showed that open Lck clusters were bigger and denser than closed Lck clusters [21]. In SMLM,
314 re-excitation of the same molecule can lead to overestimation of clustering [48]. Thus, we
315 investigated here whether Lck switches between confined and free diffusion modes. By
316 tracking single Lck molecules, we were indeed able to set a threshold to distinguish a
317 population that diffuses freely from one that exhibited restricted diffusion. We found that
318 wild-type Lck (wtLck-PAmCherry) transitioned between free and confined states in both
319 resting and stimulated T cells, strongly suggesting that the kinase has a sophisticated search
320 strategy.

bioRxiv preprint doi: https://doi.org/10.1101/446732; this version posted October 18, 2018. The copyright holder for this preprint (which was not certified by peer review) is the author/funder, who has granted bioRxiv a license to display the preprint in perpetuity. It is made available under aCC-BY-NC 4.0 International license.

In a study employing immunofluorescence staining, a pre-existing pool of constitutively active Lck was used to explain the readiness of Lck to phosphorylate the TCR immediately after T cell stimulation [22], while showing no difference in the fraction of open Lck when comparing stimulated to resting cells. Therefore, it was speculated that Lck undergoes re-distribution upon T-cell stimulation, while maintaining the same overall fraction of Lck in the open and closed conformation. By examining the diffusion modes of Lck, as a function of conformational status, we can provide an alternative explanation of how the kinase can be efficient at both searching for substrates and phosphorylating the TCR complex. Firstly, we found that T cell stimulation significantly changed the behavior of wtLck, promoting Lck molecules to spend more time in confinements, compared to resting cells. Further our results showed that in resting cells, wtLck behaved like the closed Lck mutant in both activating and resting conditions. In contrast, in stimulated cells, wtLck demonstrated a diffusion pattern that was similar to that of the open Lck mutant in both conditions. These observations led us to the conclusion that T cell activation leads to a higher proportion of open Lck, supporting the recent findings that were obtained with a fluorescence resonance energy transfer (FRET) Lck biosensor [19]. Our findings do not exclude the possibility of a pre-existing pool of open Lck.

Comparing the level of confinement of open and closed Lck mutations (Fig. S4) clearly showed that diffusion behaviour dependent on the conformational state of the enzyme. Lck^{Y394F}-PAmCherry i.e. closed Lck was confined than wtLck-PAmCherry in stimulated cells and Lck^{Y505F}-PAmCherry i.e. open Lck in stimulated and resting cells. Further, Lck^{Y394F}-PAmCherry demonstrated similar confinement to that of wtLck-PAmCherry in resting cells. The values obtained for the open mutant, both in stimulated and resting cells were closer to the value that we obtained for wtLck-PAmCherry in stimulating conditions. Taken together, our data support that notion that the open conformational state of Lck is

bioRxiv preprint doi: https://doi.org/10.1101/446732; this version posted October 18, 2018. The copyright holder for this preprint (which was not certified by peer review) is the author/funder, who has granted bioRxiv a license to display the preprint in perpetuity. It is made available under aCC-BY-NC 4.0 International license.

346 responsible for Lck confinement and that T cell activation resulted in converting some of the
347 wtLck molecules into the open state [19,20].

348 All Lck variants demonstrated some level of confinement in resting conditions. As these
349 results were obtained by expressing Lck variants in Jurkat cell lines, this confinement may be
350 an outcome of self-association with endogenous active Lck, and may be related to a pre-
351 existing pool of opened Lck in resting cells. Other mechanisms such as Lck's SH4 domain
352 interaction with lipid rafts [49,50] and microdomains [51,52] were previously suggested. Such
353 scenarios should have, however, also affected Lck10-PAmCherry, as this segment is
354 responsible for anchoring Lck to the membrane and should have resulted in slower diffusion
355 in stimulated cells. However this was not the case; similarly to closed Lck (Lck^{Y394F}-
356 PAmCherry) we found no difference in confinement of Lck10-PAmCherry in resting and
357 stimulated T cells. Further, one may hypothesize that Lck confinement is indirectly related to
358 membrane domains, by interacting with other proteins that are lipid raft-associated. However,
359 from our results with open Lck (Lck^{Y505F}-PAmCherry) we could not find support for this
360 idea, as Lck^{Y505F} was similarly confined in resting and stimulated cells.

361 The kinase-dead mutant, Lck^{K273R}-PAmCherry, was found to be minimally-confined in
362 resting and stimulated cells. It is possible that the K273R mutation in Lck prevents the
363 rearrangements in the activation loop that prevent self-association of Lck^{K273R}, or interaction
364 with other proteins, thus, limiting confinement [13]. Relying on our results obtained for wtLck-
365 PAmCherry, and thus assuming that a greater population of endogenous Lck was in the open,
366 confined state in stimulated Jurkat cells compared to resting cells, $Lck^{K273R, Y505F}$-PAmCherry
367 was found to be highly confined in stimulated cells, supporting the hypothesis that Lck self-
368 associated with other active Lck, therefore, promoting a more confined population. This is
369 consistent with a previous report on Lck self-association in the open conformation [43]. Given

bioRxiv preprint doi: https://doi.org/10.1101/446732; this version posted October 18, 2018. The copyright holder for this preprint (which was not certified by peer review) is the author/funder, who has granted bioRxiv a license to display the preprint in perpetuity. It is made available under aCC-BY-NC 4.0 International license.

370 that Lck in the open conformation exhibited confined diffusion and hyperactivity [13,14], it is
371 highly likely that this state results in high local phosphorylation rates.

372 In conclusion, we provide evidence that the conformation of Lck was the main driver of Lck
373 diffusion modes with open Lck causing confined diffusion and closed Lck enabling free
374 diffusion. Individual Lck molecules can switch between confined and free diffusion in resting
375 and stimulated T cells. This is consistent with a dual-state search strategy that enables Lck to
376 scan large areas of the membrane in the closed state, but efficiently phosphorylate TCR-CD3
377 complexes at numerous sites in the open state.

378

bioRxiv preprint doi: https://doi.org/10.1101/446732; this version posted October 18, 2018. The copyright holder for this preprint (which was not certified by peer review) is the author/funder, who has granted bioRxiv a license to display the preprint in perpetuity. It is made available under aCC-BY-NC 4.0 International license.

Methods and Materials

Plasmids

Lck and Lck10 were amplified by PCR and inserted within the Ecot1 and Age1 restriction sites of a pPAmCherry-N1 plasmid. Y394F, Y505F and K273R mutations were further introduced via site-directed mutagenesis.

Sample Preparation

Jurkat cells were cultured in RPMI medium (Gibco) containing phenol-red and supplemented with 10% (vol/vol) FBS, 2 mM L-glutamine (Invitrogen), 1 mM penicillin (Invitrogen) and 1 mM streptomycin (Invitrogen). Cell cultures were passaged normally every ~48 hours, when the cell count reached ~$8x10^5$ viable cells per ml. The cells were cultured for at least 1 week (3-4 passages) after thawing prior to transfection and imaging. No cells were used after passage 20.

Cells were transfected by electroporation (Neon; Invitrogen); briefly, cells were collected before reaching a cell density of 8×10^5 cell/ml and while ≥90% viable. The cells were washed twice with 1x PBS in 37°C and resuspended in the resuspension buffer (R-buffer) provided with the Neon kit. Three pulses of 1325 V with 10 ms duration were applied. The cells were allowed to recover in clear RPMI 1640 medium (Gibco) supplemented with 20% HI-FBS for overnight. Prior to imaging, fresh warm (37°C) media with 40 mM HEPES, pH 7.4 was added to achieve a final concentration of 20 mM HEPES.

1.5H coverslips (Marienfeld-Superior) were waterbath-sonicated in four 30-minutes stages: 1 M KOH, Acetone, EtOH and ultra-pure (18 MΩ) water. The coverslips were then allowed to adsorb 0.01% PLL (Sigma) in ultra-pure water for 15 minutes. Excess solution was later aspirated and the coverslips were baked-dry in 60 °C for 1 hour. Finally, after cooling-down,

bioRxiv preprint doi: https://doi.org/10.1101/446732; this version posted October 18, 2018. The copyright holder for this preprint (which was not certified by peer review) is the author/funder, who has granted bioRxiv a license to display the preprint in perpetuity. It is made available under aCC-BY-NC 4.0 International license.

the coverslips were coated with either 0.01 mg/ml anti-CD3 (OKT3; eBioscience) and 0.01 mg/ml anti-CD28 (CD28.2; Invitrogen) for stimulating conditions or 0.01 mg/ml αCD90 for (Thy-1; eBioscience) for resting conditions and let rest in 4°C overnight before imaging. The coverslips were washed 3 times with phosphate buffer saline (PBS) pre-warmed to 37°C before the cells were transferred onto them to interact with the antibodies. For live-cell experiments, imaging took place ~5 minutes after cell-transfer, or fixed with 4% paraformaldehyde (P6148; Sigma) in 37°C, followed by 3 washing cycles with PBS for fixed-cell imaging.

Imaging

For each sptPALM experiment 10,000 frames were acquired in a ~50 frames per second (18 ms exposure time) rate on a total internal reflection fluorescence (TIRF) microscope (ELYRA, Zeiss) in 37 °C using a 100× oil immersion objective (N.A. = 1.46) and a 67.5° incident beam angle. PAmCherry fused to Lck variants were continuously photoactivated using a 405 nm laser radiation tuned to 0.5-5 μW (interchangeable during acquisition to maintain a low density) and continuously excited with a 561 nm laser tuned to 2.5 mW. Point density was monitored by using ZEN (Zeiss) online-processing tool.

Data Analysis

All accumulated data are comprised of three biologically-independent experiments, i.e. each mutant was imaged in two or more cells (in one of the three repetitions, where a repetition relates to a different transfection) in each cell-activation state (stimulated or resting). We used Diatrack [53] for fitting the point spread functions (PSFs) to a Gaussian with a 1.75 pixel width (1 pixel ≈ 0.097 nm) and then to track the particles by setting the search radius to 10 pixels.

bioRxiv preprint doi: https://doi.org/10.1101/446732; this version posted October 18, 2018. The copyright holder for this preprint (which was not certified by peer review) is the author/funder, who has granted bioRxiv a license to display the preprint in perpetuity. It is made available under aCC-BY-NC 4.0 International license.

The data was later analyzed by a custom MATLAB (Mathworks) adaptation of the trajectory analysis part of a previously published multi-target tracing (MTT) code [32]. Immobile particles (RMSD < 2 pixels) and trajectories shorter than 15 frames were excluded from analysis. Stages of confined and free diffusion were detected according to equation 1, with D_{free} = 2.15 μm^2/sec (Fig. S2b, bottom), W = 4 and t_W was the sum of the exposure time and the CCD reading time (~19.7 ms). To detect time spent in confinement, each sequence was segmented to non-overlapping windows of 5 frames and in each block of 5 frames, the ratio of confined:total particles was calculated. Each value of one 5 frames-window is a count in the histogram. All data processing and statistical analyses were performed in MATLAB.

Statistical Tests

To compare between two populations of confinement fractions, that do not normally distribute, we used the Mann-Whitney U test, while the Kruskal-Wellis test was used for multiple datasets followed by a bonferroni post-hoc test. **** and n.s. indicate $p \leq 0.00001$ and $p > 0.01$, respectively. Ranges around median and mean values in supplementary text are the 95% confidence intervals calculated from bootstrapping the data by sampling 10,000 times.

bioRxiv preprint doi: https://doi.org/10.1101/446732; this version posted October 18, 2018. The copyright holder for this preprint (which was not certified by peer review) is the author/funder, who has granted bioRxiv a license to display the preprint in perpetuity. It is made available under aCC-BY-NC 4.0 International license.

450 **Supplementary Materials**

451 **Fig.S1** Relationship between Lck diffusion coefficient and confinement

452 **Fig.S2** Diffusion coefficients histograms of wtLck, Lck10, LckY505F, LckY394F,
453 LckK273R and LckK273R, Y505F in stimulated and resting Jurkat cells

454 **Fig.S3** Illustration of confinement ratio analysis

455 **Fig.S4** Comparison of confinement analysis result

456 **Fig.S5** Comparison of confinement analysis result of wtLck-PAmCherry, LckK273R-
457 PAmCherry and LckK273R, Y505F-PAmCherry in stimulated and resting cells

458 **Movie S1**

459 **Movie S2**

460 **Movie S3**

461 **Movie S4**

462 **Movie S5**

463

464

465

466

467

bioRxiv preprint doi: https://doi.org/10.1101/446732; this version posted October 18, 2018. The copyright holder for this preprint (which was not certified by peer review) is the author/funder, who has granted bioRxiv a license to display the preprint in perpetuity. It is made available under aCC-BY-NC 4.0 International license.

References and Notes:

1 Klammt, C. & Lillemeier, B. F. How membrane structures control T cell signaling. *Front Immunol* **3**, 291, doi:10.3389/fimmu.2012.00291 (2012).

2 Guy, C. S. & Vignali, D. A. Organization of proximal signal initiation at the TCR:CD3 complex. *Immunol Rev* **232**, 7-21, doi:10.1111/j.1600-065X.2009.00843.x (2009).

3 Dustin, M. L. The immunological synapse. *Cancer Immunol Res* **2**, 1023-1033, doi:10.1158/2326-6066.CIR-14-0161 (2014).

4 Carreno, L. J. *et al.* T-cell antagonism by short half-life pMHC ligands can be mediated by an efficient trapping of T-cell polarization toward the APC. *Proc Natl Acad Sci U S A* **107**, 210-215, doi:10.1073/pnas.0911258107 (2010).

5 van der Merwe, P. A., Zhang, H. & Cordoba, S. P. Why do some T cell receptor cytoplasmic domains associate with the plasma membrane? *Front Immunol* **3**, 29, doi:10.3389/fimmu.2012.00029 (2012).

6 Rossy, J., Williamson, D. J. & Gaus, K. How does the kinase Lck phosphorylate the T cell receptor? Spatial organization as a regulatory mechanism. *Front Immunol* **3**, 167, doi:10.3389/fimmu.2012.00167 (2012).

7 Weiss, A. T cell antigen receptor signal transduction: a tale of tails and cytoplasmic protein-tyrosine kinases. *Cell* **73**, 209-212 (1993).

8 Kabouridis, P. S., Magee, A. I. & Ley, S. C. S-acylation of LCK protein tyrosine kinase is essential for its signalling function in T lymphocytes. *EMBO J* **16**, 4983-4998, doi:10.1093/emboj/16.16.4983 (1997).

9 Yurchak, L. K. & Sefton, B. M. Palmitoylation of either Cys-3 or Cys-5 is required for the biological activity of the Lck tyrosine protein kinase. *Mol Cell Biol* **15**, 6914-6922 (1995).

10 Li, L. *et al.* Ionic CD3-Lck interaction regulates the initiation of T-cell receptor signaling. *Proc Natl Acad Sci U S A* **114**, E5891-E5899, doi:10.1073/pnas.1701990114 (2017).

11 Briese, L. & Willbold, D. Structure determination of human Lck unique and SH3 domains by nuclear magnetic resonance spectroscopy. *BMC Structural Biology* **3**, 3, doi:10.1186/1472-6807-3-3 (2003).

12 Casas, J. *et al.* Ligand-engaged TCR is triggered by Lck not associated with CD8 coreceptor. *Nature Communications* **5**, 5624, doi:10.1038/ncomms6624 (2014).

13 Liaunardy-Jopeace, A., Murton, B. L., Mahesh, M., Chin, J. W. & James, J. R. Encoding optical control in LCK kinase to quantitatively investigate its activity in live cells. *Nat Struct Mol Biol* **24**, 1155-1163, doi:10.1038/nsmb.3492 (2017).

14 Hui, E. & Vale, R. D. In vitro membrane reconstitution of the T-cell receptor proximal signaling network. *Nat Struct Mol Biol* **21**, 133-142, doi:10.1038/nsmb.2762 (2014).

15 Nika, K. *et al.* A weak Lck tail bite is necessary for Lck function in T cell antigen receptor signaling. *J Biol Chem* **282**, 36000-36009, doi:10.1074/jbc.M702779200 (2007).

16 Gervais, F. G., Chow, L. M., Lee, J. M., Branton, P. E. & Veillette, A. The SH2 domain is required for stable phosphorylation of p56lck at tyrosine 505, the negative regulatory site. *Mol Cell Biol* **13**, 7112-7121 (1993).

17 Davis, S. J. & van der Merwe, P. A. Lck and the nature of the T cell receptor trigger. *Trends in Immunology* **32**, 1-5, doi:https://doi.org/10.1016/j.it.2010.11.003 (2011).

18 Douglass, A. D. & Vale, R. D. Single-molecule microscopy reveals plasma membrane microdomains created by protein-protein networks that exclude or trap signaling molecules in T cells. *Cell* **121**, 937-950, doi:10.1016/j.cell.2005.04.009 (2005).

19 Philipsen, L. *et al.* De novo phosphorylation and conformational opening of the tyrosine kinase Lck act in concert to initiate T cell receptor signaling. *Sci Signal* **10**, doi:10.1126/scisignal.aaf4736 (2017).

bioRxiv preprint doi: https://doi.org/10.1101/446732; this version posted October 18, 2018. The copyright holder for this preprint (which was not certified by peer review) is the author/funder, who has granted bioRxiv a license to display the preprint in perpetuity. It is made available under aCC-BY-NC 4.0 International license.

20 Stirnweiss, A. *et al.* T cell activation results in conformational changes in the Src family kinase Lck to induce its activation. *Sci Signal* **6**, ra13, doi:10.1126/scisignal.2003607 (2013).

21 Rossy, J., Owen, D. M., Williamson, D. J., Yang, Z. & Gaus, K. Conformational states of the kinase Lck regulate clustering in early T cell signaling. *Nat Immunol* **14**, 82-89, doi:10.1038/ni.2488 (2013).

22 Nika, K. *et al.* Constitutively active Lck kinase in T cells drives antigen receptor signal transduction. *Immunity* **32**, 766-777, doi:10.1016/j.immuni.2010.05.011 (2010).

23 Ballek, O., Valecka, J., Manning, J. & Filipp, D. The pool of preactivated Lck in the initiation of T-cell signaling: a critical re-evaluation of the Lck standby model. *Immunol Cell Biol* **93**, 384-395, doi:10.1038/icb.2014.100 (2015).

24 Paster, W. *et al.* Genetically encoded Forster resonance energy transfer sensors for the conformation of the Src family kinase Lck. *J Immunol* **182**, 2160-2167, doi:10.4049/jimmunol.0802639 (2009).

25 Moogk, D. *et al.* Constitutive Lck Activity Drives Sensitivity Differences between CD8+ Memory T Cell Subsets. *J Immunol* **197**, 644-654, doi:10.4049/jimmunol.1600178 (2016).

26 Bénichou, O., Loverdo, C., Moreau, M. & Voituriez, R. Intermittent search strategies. *Reviews of Modern Physics* **83**, 81-129 (2011).

27 Ike, H. *et al.* Mechanism of Lck recruitment to the T-cell receptor cluster as studied by single-molecule-fluorescence video imaging. *Chemphyschem* **4**, 620-626, doi:10.1002/cphc.200300670 (2003).

28 Ballek, O. *et al.* TCR Triggering Induces the Formation of Lck-RACK1-Actinin-1 Multiprotein Network Affecting Lck Redistribution. *Front Immunol* **7**, 449, doi:10.3389/fimmu.2016.00449 (2016).

29 Fernandes, R. A. *et al.* Constraining CD45 exclusion at close-contacts provides a mechanism for discriminatory T-cell receptor signalling. *bioRxiv*, doi:10.1101/109785 (2017).

30 Manley, S. *et al.* High-density mapping of single-molecule trajectories with photoactivated localization microscopy. *Nat Methods* **5**, 155-157, doi:10.1038/nmeth.1176 (2008).

31 Subach, F. V. *et al.* Photoactivatable mCherry for high-resolution two-color fluorescence microscopy. *Nat Methods* **6**, 153-159, doi:10.1038/nmeth.1298 (2009).

32 Serge, A., Bertaux, N., Rigneault, H. & Marguet, D. Dynamic multiple-target tracing to probe spatiotemporal cartography of cell membranes. *Nat Methods* **5**, 687-694, doi:10.1038/nmeth.1233 (2008).

33 Ma, Y. *et al.* An intermolecular FRET sensor detects the dynamics of T cell receptor clustering. *Nat Commun* **8**, 15100, doi:10.1038/ncomms15100 (2017).

34 Gaus, K., Chklovskaia, E., Fazekas de St Groth, B., Jessup, W. & Harder, T. Condensation of the plasma membrane at the site of T lymphocyte activation. *J Cell Biol* **171**, 121-131, doi:10.1083/jcb.200505047 (2005).

35 Ledbetter, J. A. *et al.* CD4, CD8 and the role of CD45 in T-cell activation. *Current Opinion in Immunology* **5**, 334-340, doi:https://doi.org/10.1016/0952-7915(93)90050-3 (1993).

36 Simeoni, L. Lck activation: puzzling the pieces together. *Oncotarget* **8**, 102761-102762, doi:10.18632/oncotarget.22309 (2017).

37 Laham, L. E., Mukhopadhyay, N. & Roberts, T. M. The activation loop in Lck regulates oncogenic potential by inhibiting basal kinase activity and restricting substrate specificity. *Oncogene* **19**, 3961-3970, doi:10.1038/sj.onc.1203738 (2000).

38 Chakraborty, A. K. & Weiss, A. Insights into the initiation of TCR signaling. *Nat Immunol* **15**, 798-807, doi:10.1038/ni.2940 (2014).

39 D'Oro, U., Sakaguchi, K., Appella, E. & Ashwell, J. D. Mutational analysis of Lck in CD45-negative T cells: dominant role of tyrosine 394 phosphorylation in kinase activity. *Mol Cell Biol* **16**, 4996-5003 (1996).

40 Courtney, A. H. *et al.* A Phosphosite within the SH2 Domain of Lck Regulates Its Activation by CD45. *Mol Cell* **67**, 498-511 e496, doi:10.1016/j.molcel.2017.06.024 (2017).

bioRxiv preprint doi: https://doi.org/10.1101/446732; this version posted October 18, 2018. The copyright holder for this preprint (which was not certified by peer review) is the author/funder, who has granted bioRxiv a license to display the preprint in perpetuity. It is made available under aCC-BY-NC 4.0 International license.

41 Dobbins, J. *et al.* Binding of the cytoplasmic domain of CD28 to the plasma membrane inhibits Lck recruitment and signaling. *Sci Signal* **9**, ra75, doi:10.1126/scisignal.aaf0626 (2016).
42 Filipp, D. *et al.* Lck-dependent Fyn activation requires C terminus-dependent targeting of kinase-active Lck to lipid rafts. *J Biol Chem* **283**, 26409-26422, doi:10.1074/jbc.M710372200 (2008).
43 Kapoor-Kaushik, N. *et al.* Distinct Mechanisms Regulate Lck Spatial Organization in Activated T Cells. *Front Immunol* **7**, 83, doi:10.3389/fimmu.2016.00083 (2016).
44 Sheng, R. *et al.* Lipids Regulate Lck Protein Activity through Their Interactions with the Lck Src Homology 2 Domain. *J Biol Chem* **291**, 17639-17650, doi:10.1074/jbc.M116.720284 (2016).
45 Gorfe, A. A., Lu, B., Yu, Z. & McCammon, J. A. Enzymatic activity versus structural dynamics: the case of acetylcholinesterase tetramer. *Biophys J* **97**, 897-905, doi:10.1016/j.bpj.2009.05.033 (2009).
46 Merlino, A. *et al.* The importance of dynamic effects on the enzyme activity: X-ray structure and molecular dynamics of onconase mutants. *J Biol Chem* **280**, 17953-17960, doi:10.1074/jbc.M501339200 (2005).
47 Hanson, J. A. *et al.* Illuminating the mechanistic roles of enzyme conformational dynamics. *Proc Natl Acad Sci U S A* **104**, 18055-18060, doi:10.1073/pnas.0708600104 (2007).
48 Baumgart, F. *et al.* Varying label density allows artifact-free analysis of membrane-protein nanoclusters. *Nat Methods* **13**, 661-664, doi:10.1038/nmeth.3897 (2016).
49 Jordan, S. & Rodgers, W. T cell glycolipid-enriched membrane domains are constitutively assembled as membrane patches that translocate to immune synapses. *J Immunol* **171**, 78-87 (2003).
50 Ventimiglia, L. N. & Alonso, M. A. The role of membrane rafts in Lck transport, regulation and signalling in T-cells. *Biochem J* **454**, 169-179, doi:10.1042/BJ20130468 (2013).
51 Ilangumaran, S., Arni, S., van Echten-Deckert, G., Borisch, B. & Hoessli, D. C. Microdomain-dependent regulation of Lck and Fyn protein-tyrosine kinases in T lymphocyte plasma membranes. *Mol Biol Cell* **10**, 891-905 (1999).
52 Filipp, D., Ballek, O. & Manning, J. Lck, Membrane Microdomains, and TCR Triggering Machinery: Defining the New Rules of Engagement. *Front Immunol* **3**, 155, doi:10.3389/fimmu.2012.00155 (2012).
53 Vallotton, P. & Olivier, S. Tri-track: free software for large-scale particle tracking. *Microsc Microanal* **19**, 451-460, doi:10.1017/S1431927612014328 (2013).

Funding: K.G. acknowledges funding from the ARC Centre of Excellence in Advanced Molecular Imaging (CE140100011), Australian Research Council (LP140100967 and DP130100269) and National Health and Medical Research Council of Australia (1059278 and 1037320).

Author Contributions: GH performed experiments, modified analysis, analyzed data, and wrote manuscript. EP established analysis and helped write the manuscript. ZY was responsible for the generation of Lck constructs. DJN and JG aided in writing and drafting of

bioRxiv preprint doi: https://doi.org/10.1101/446732; this version posted October 18, 2018. The copyright holder for this preprint (which was not certified by peer review) is the author/funder, who has granted bioRxiv a license to display the preprint in perpetuity. It is made available under aCC-BY-NC 4.0 International license.

608 the manuscript. JR provided guidance with experiments. KG designed the project,

609 interpreted the data and wrote the manuscript.

610 **Competing interests:** The authors declare no competing interests.

611

bioRxiv preprint doi: https://doi.org/10.1101/446732; this version posted October 18, 2018. The copyright holder for this preprint (which was not certified by peer review) is the author/funder, who has granted bioRxiv a license to display the preprint in perpetuity. It is made available under aCC-BY-NC 4.0 International license.

612 **Figures:**

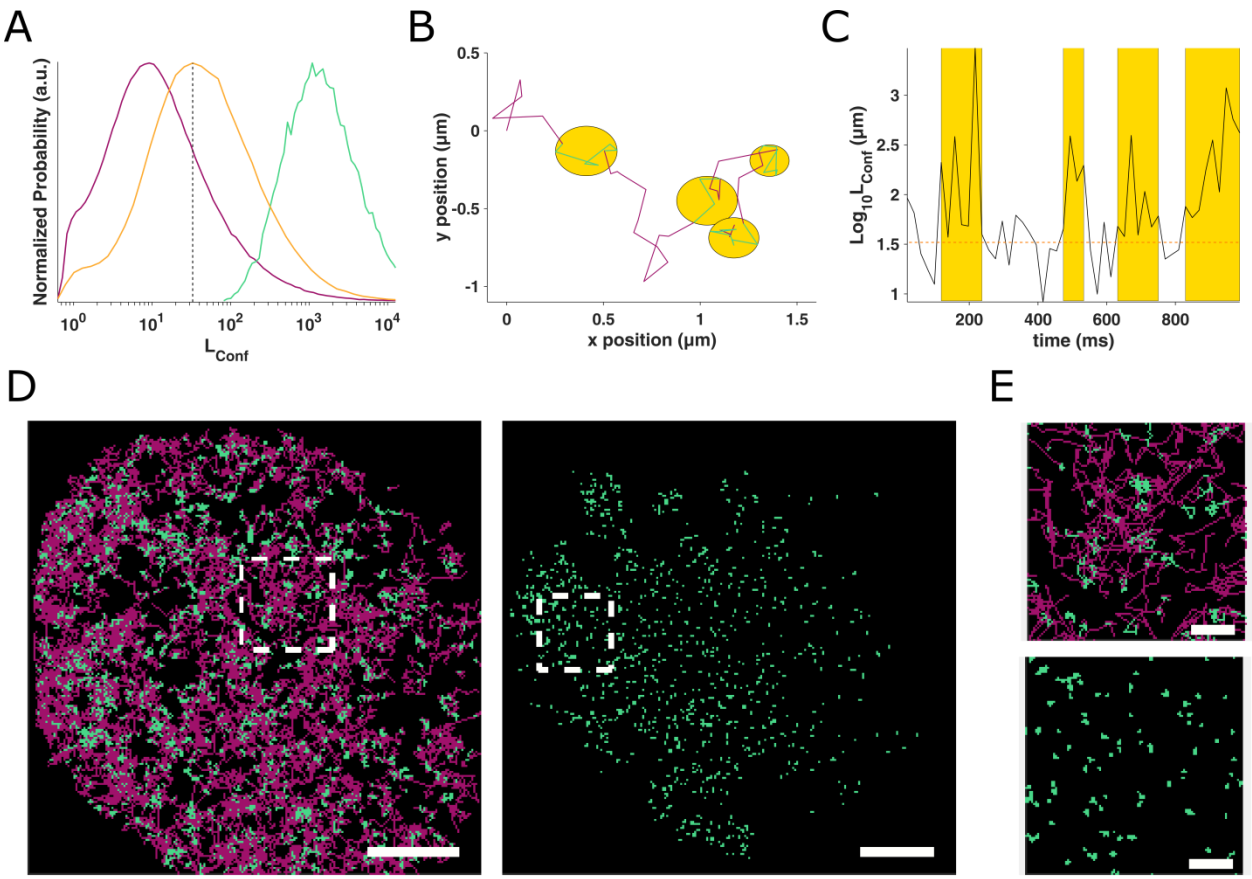

613

614 **Fig.1 wtLck switches between free and confined states**. **(A)** L_{Conf} acquired for Lck10-
615 PAmCherry in resting Jurkat cells (purple), wtLck-PAmCherry in stimulated Jurkat cells
616 (orange) and wtLck-PAmCherry in fixed cells (cyan), normalized to peak value. The dashed
617 vertical line marks the threshold where a particle was to be considered confined, i.e., if it had
618 three or more consecutive steps with an L_{Conf} value greater than that threshold. **(B)** An
619 experimental trajectory decomposed to free (magenta) and confined (cyan) states, with the
620 confinements highlighted in yellow circles. **(C)** Time evolution of L_{Conf} values for the
621 trajectory in (B) with the threshold marked with an orange dashed line and the confined
622 periods with a yellow shade. **(D)** Trajectory decomposition maps of wtLck-PAmCherry in a
623 stimulated live cells (left) and fixed Jurkat cells (right) Free periods are colored magenta,

bioRxiv preprint doi: https://doi.org/10.1101/446732; this version posted October 18, 2018. The copyright holder for this preprint (which was not certified by peer review) is the author/funder, who has granted bioRxiv a license to display the preprint in perpetuity. It is made available under aCC-BY-NC 4.0 International license.

624 whereas confined periods are colored cyan. Scale bar = 5 µm. **(E)** 5 µm by 5 µm zoomed-in

625 regions of interest in (D) (top – live, bottom - fixed). Scale bar = 1 µm.

626

bioRxiv preprint doi: https://doi.org/10.1101/446732; this version posted October 18, 2018. The copyright holder for this preprint (which was not certified by peer review) is the author/funder, who has granted bioRxiv a license to display the preprint in perpetuity. It is made available under aCC-BY-NC 4.0 International license.

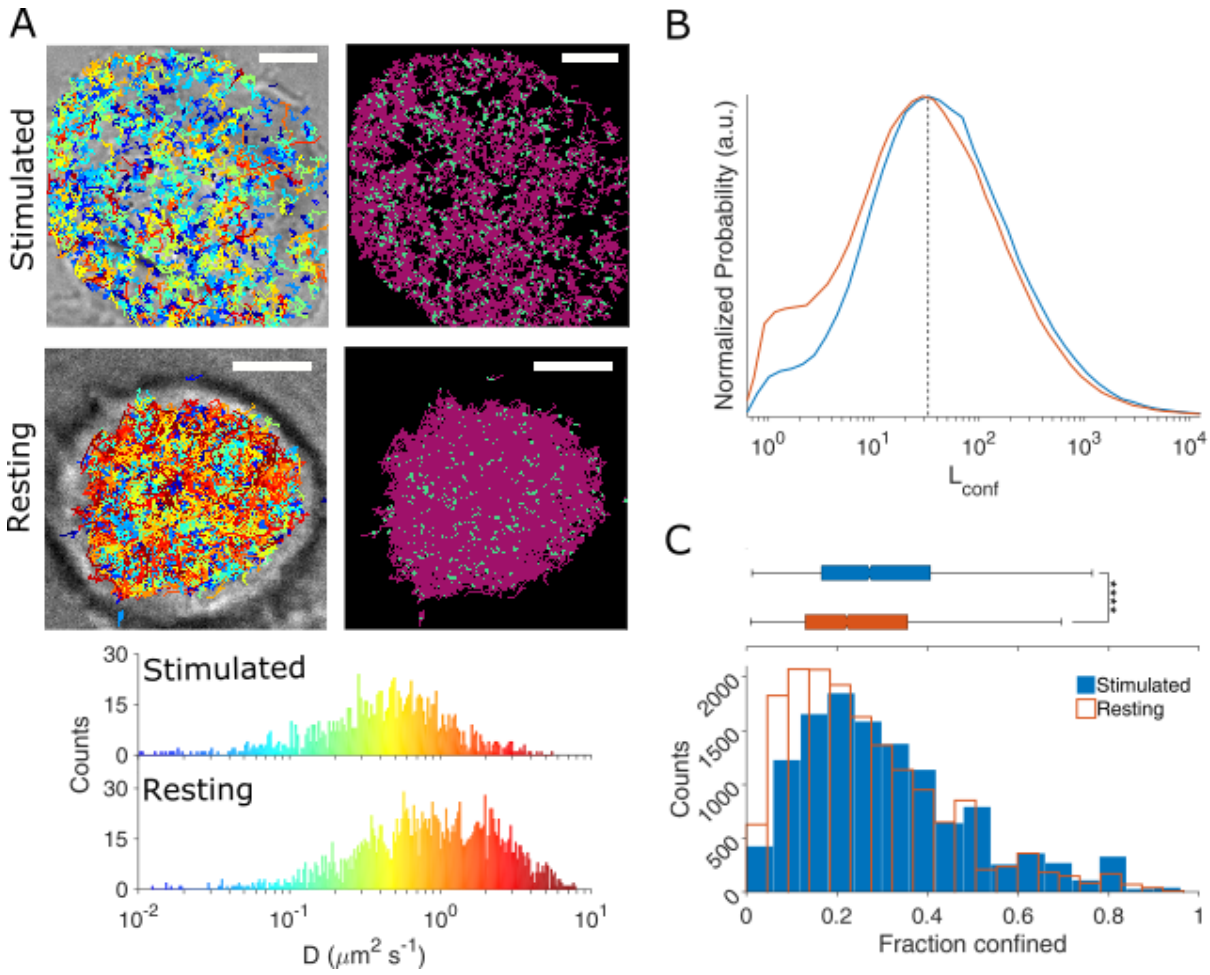

Fig.2 wtLck-PAmCherry is more confined in stimulated cells. **(A)** Representative stimulated and resting Jurkat E6-1 cells expressing wtLck-PAmCherry. The left panels show bright field images of the cells with detected trajectories overlaid, color-coded according to their initial diffusion. The right panels show the free (magenta) and confined (cyan) modes of diffusion. Scale bar = 5 µm. Bottom: diffusions histogram corresponding to the cells above, sharing mutual color-coding. **(B)** L_{Conf} histograms for wtLck-PAmCherry in resting (orange) and stimulated (blue) cells. **(C)** Histograms of the fraction of confined wtLck-PAmCherry molecules obtained for 13 stimulated (blue) and 17 resting (orange) Jurkat cells. Box plot shows the median. Notch 95% confidence interval, box edges first and third quartile, lines Tukey's fences, **** $p \leq 0.00001$.

bioRxiv preprint doi: https://doi.org/10.1101/446732; this version posted October 18, 2018. The copyright holder for this preprint (which was not certified by peer review) is the author/funder, who has granted bioRxiv a license to display the preprint in perpetuity. It is made available under aCC-BY-NC 4.0 International license.

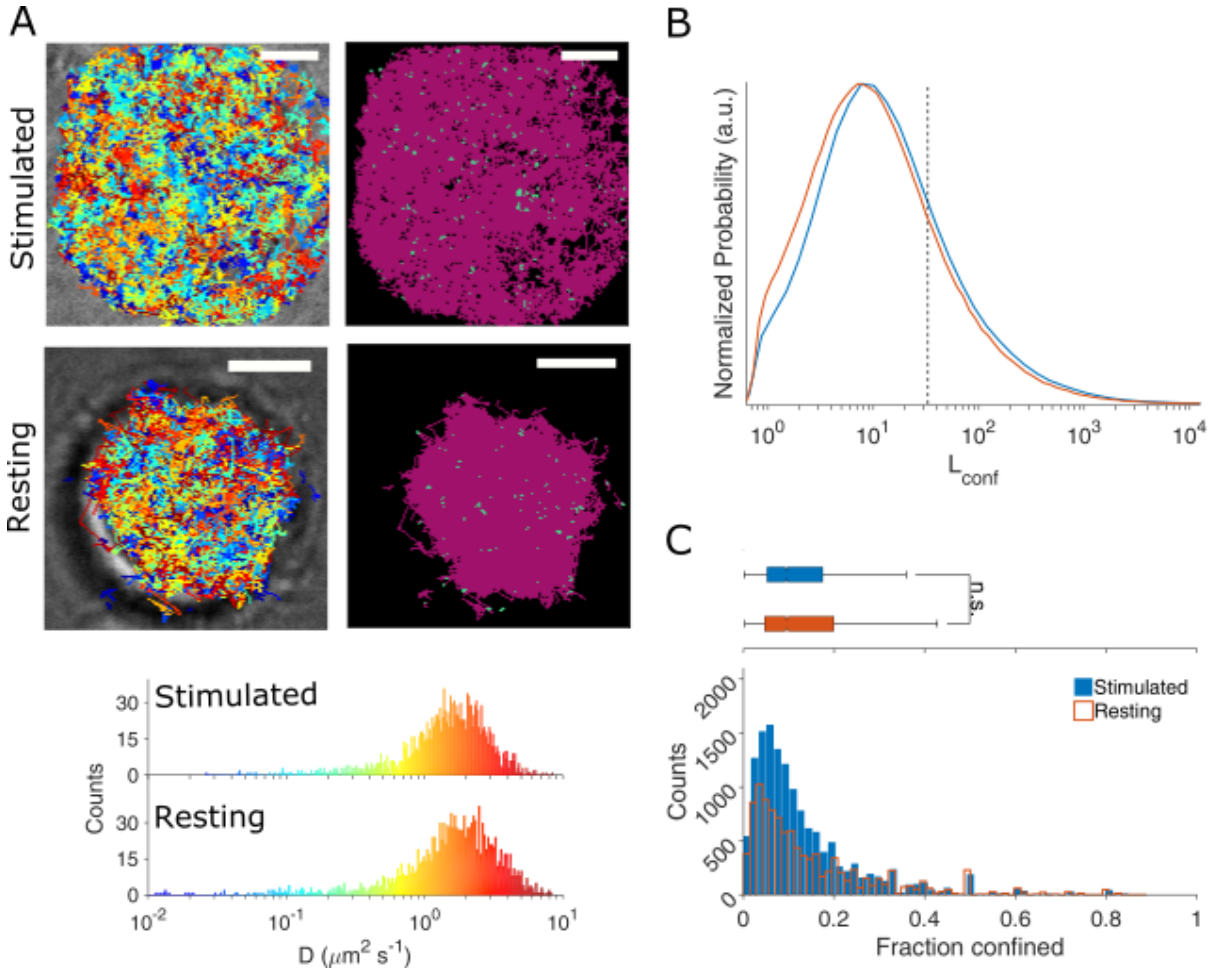

Fig. 3 Lck10-PAmCherry demonstrates free-diffusion in resting and stimulated calls. **(A)** Representative stimulated and resting Jurkat E6-1 cells expressing Lck10-PAmCherry. The left panels show bright field images of the cells with detected trajectories overlaid, color-coded according to their initial diffusion. The right panels show the free (magenta) and confined (cyan) modes of diffusion. Scale bar = 5 µm. Bottom: diffusions histogram corresponding to the cells above, sharing mutual color-coding. **(B)** L_{Conf} histograms for Lck10-PAmCherry in resting (orange) and stimulated (blue) cells. **(C)** Histograms of the fraction of confined Lck10-PAmCherry molecules obtained for 19 stimulated (blue) and 15 resting (orange) Jurkat cells. Box plot shows the median. Notch 95% confidence interval, box edges first and third quartile, lines Tukey's fences, n.s. p>0.01.

bioRxiv preprint doi: https://doi.org/10.1101/446732; this version posted October 18, 2018. The copyright holder for this preprint (which was not certified by peer review) is the author/funder, who has granted bioRxiv a license to display the preprint in perpetuity. It is made available under aCC-BY-NC 4.0 International license.

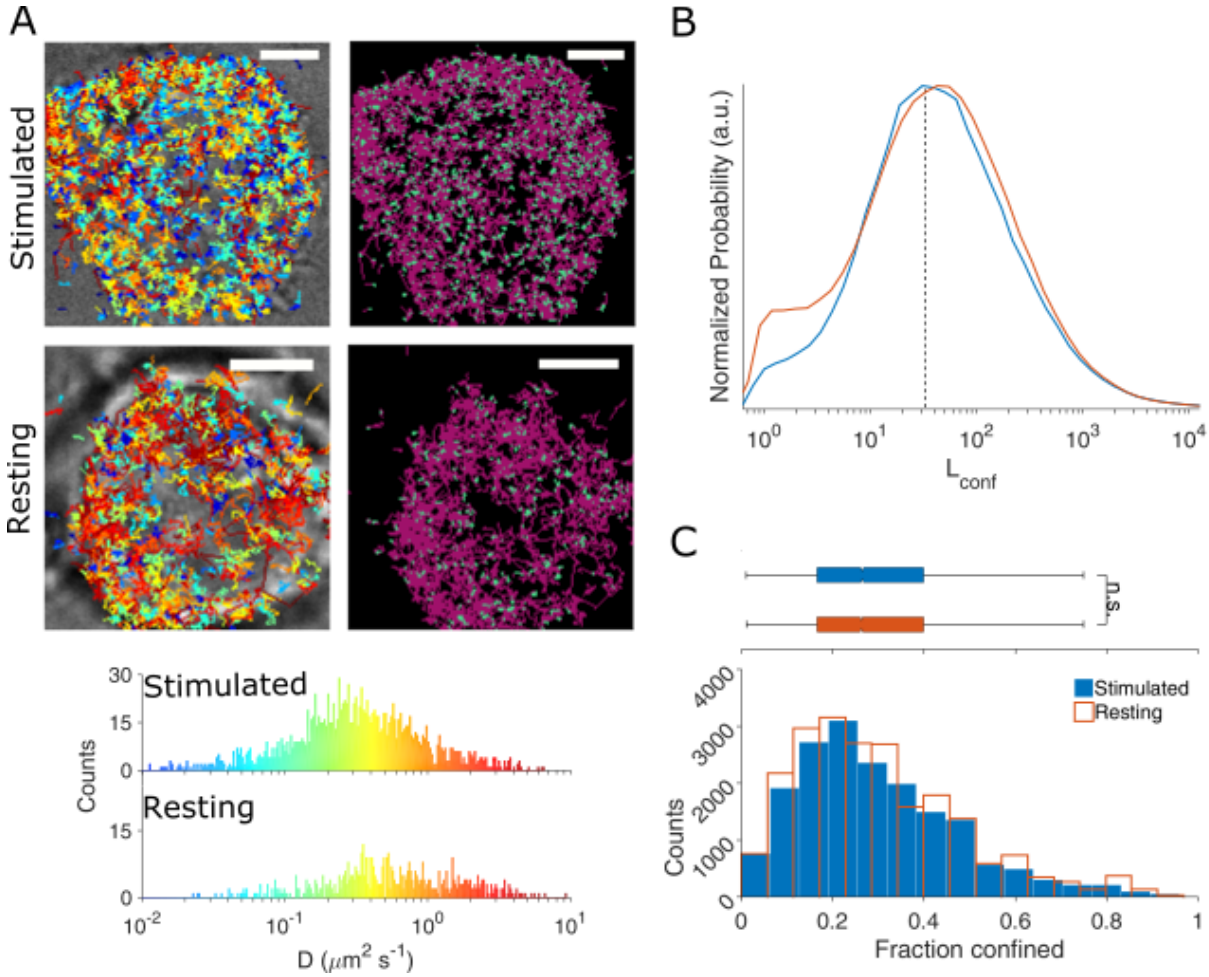

Fig. 4 Lck^{Y505F}-PAmCherry is equally confined in stimulated and resting cells. **(A)** Representative stimulated and resting Jurkat E6-1 cells expressing Lck^{Y505F}-PAmCherry. The left panels show bright field images of the cells with detected trajectories overlaid, color-coded according to their initial diffusion. The right panels show the free (magenta) and confined (cyan) modes of diffusion. Scale bar = 5 µm. Bottom: diffusions histogram corresponding to the cells above, sharing mutual color-coding. **(B)** L_{Conf} histograms for Lck^{Y505F}-PAmCherry in resting (orange) and stimulated (blue) cells. **(C)** Histograms of the fraction of confined Lck^{Y505F}-PAmCherry molecules obtained for 14 stimulated (blue) and 18

bioRxiv preprint doi: https://doi.org/10.1101/446732; this version posted October 18, 2018. The copyright holder for this preprint (which was not certified by peer review) is the author/funder, who has granted bioRxiv a license to display the preprint in perpetuity. It is made available under aCC-BY-NC 4.0 International license.

665 resting (orange) Jurkat cells. Box plot shows the median. Notch 95% confidence interval, box
666 edges first and third quartile, lines Tukey's fences, n.s. p>0.01.

667

668

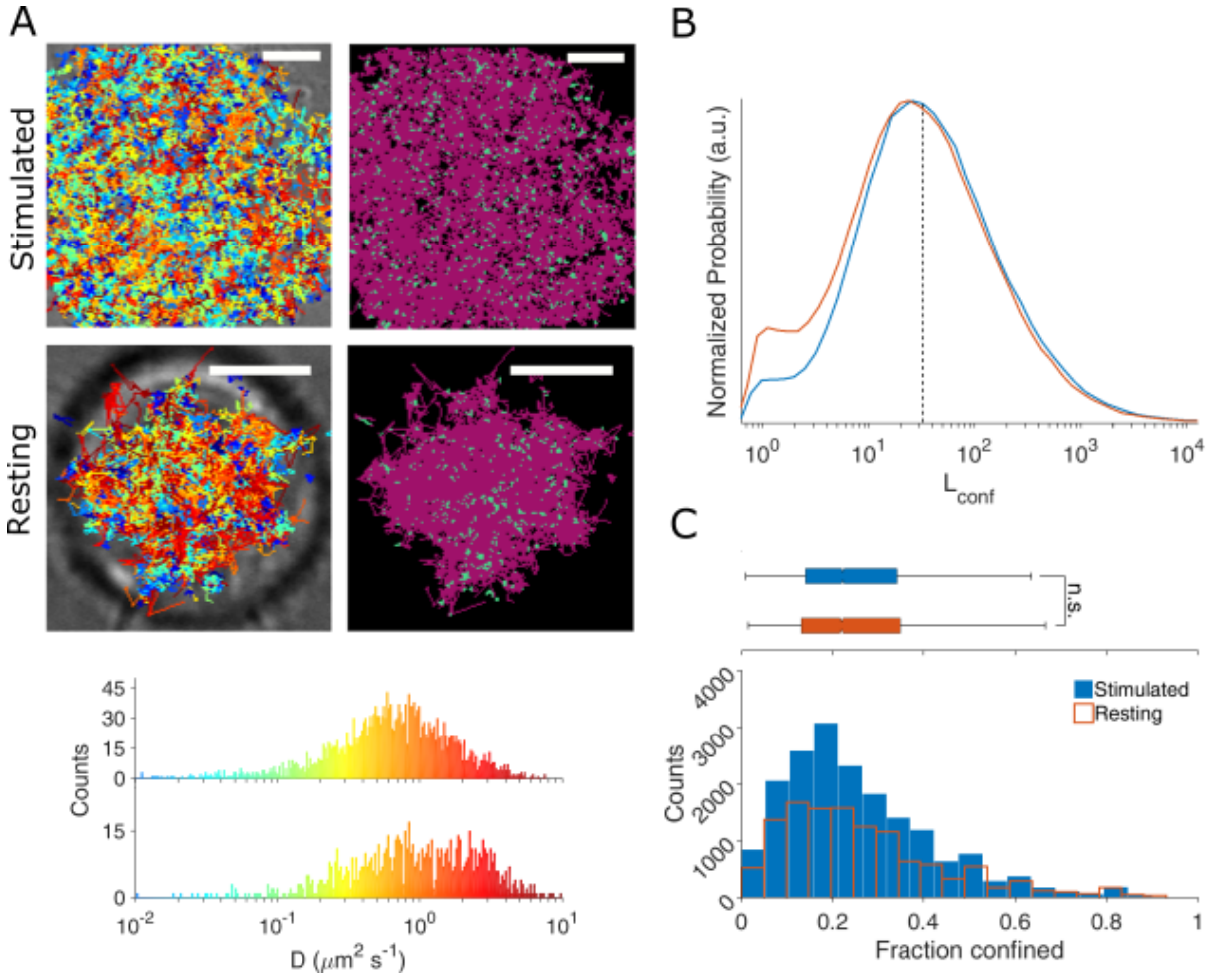

669

670

671 **Fig. 5 Lck^{Y394F}-PAmCherry is equally confined in stimulated and resting cells. (A)**
672 Representative stimulated and resting Jurkat E6-1 cells expressing Lck^{Y394F}-PAmCherry. The
673 left panels show bright field images of the cells with detected trajectories overlaid, color-
674 coded according to their initial diffusion. The right panels show the free (magenta) and
675 confined (cyan) modes of diffusion. Scale bar = 5 µm. Bottom: diffusions histogram
676 corresponding to the cells above, sharing mutual color-coding. **(B)** L_{Conf} histograms for
677 Lck^{Y394F}-PAmCherry in resting (orange) and stimulated (blue) cells. **(C)** Histograms of the

bioRxiv preprint doi: https://doi.org/10.1101/446732; this version posted October 18, 2018. The copyright holder for this preprint (which was not certified by peer review) is the author/funder, who has granted bioRxiv a license to display the preprint in perpetuity. It is made available under aCC-BY-NC 4.0 International license.

678 fraction of confined Lck^{Y394F}-PAmCherry molecules obtained for 16 stimulated (blue) and 14
679 resting (orange) Jurkat cells. Box plot shows the median. Notch 95% confidence interval, box
680 edges first and third quartile, lines Tukey's fences, n.s. $p>0.01$.

681

bioRxiv preprint doi: https://doi.org/10.1101/446732; this version posted October 18, 2018. The copyright holder for this preprint (which was not certified by peer review) is the author/funder, who has granted bioRxiv a license to display the preprint in perpetuity. It is made available under aCC-BY-NC 4.0 International license.

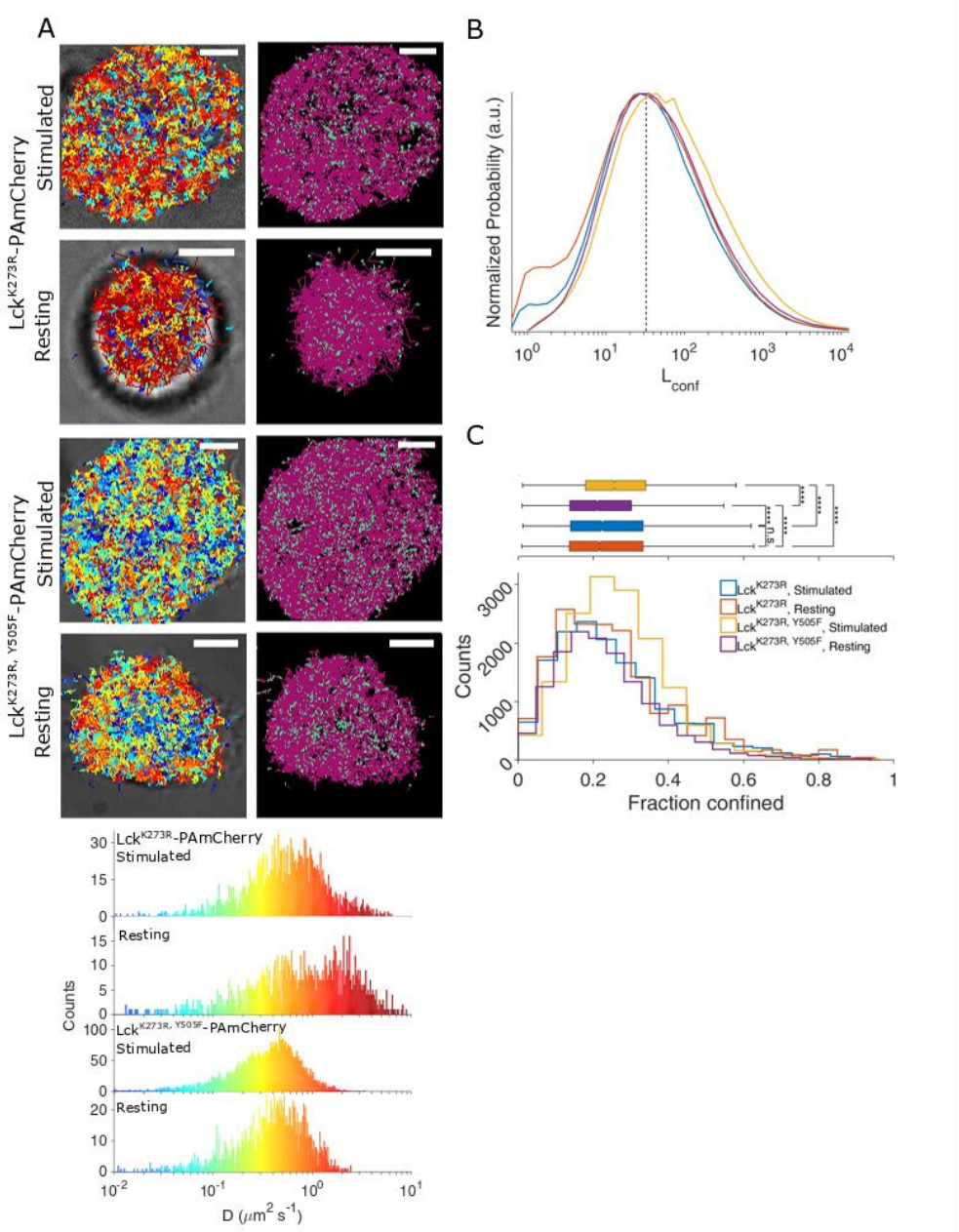

Fig. 6 Confinement analyses for Lck^{K273R}-PAmCherry and Lck$^{K273R,\ Y505F}$-PAmCherry in stimulated and resting cells. **(A)** Representative stimulated and resting Jurkat E6-1 cells expressing Lck^{K273R}-PAmCherry and Lck$^{K273R,\ Y505F}$-PAmCherry. The left panels show bright field images of the cells with detected trajectories overlaid, color-coded according to their initial diffusion. The right panels show the free (magenta) and confined (cyan) modes of diffusion. Scale bar = 5 µm. Bottom: diffusions histogram corresponding to the cells above, sharing mutual color-coding. **(B)** L_{Conf} histograms for Lck^{K273R}-PAmCherry and Lck$^{K273R,\ Y505F}$-PAmCherry in and stimulated cells. (orange, blue, purple and yellow, respectively). **(C)**

bioRxiv preprint doi: https://doi.org/10.1101/446732; this version posted October 18, 2018. The copyright holder for this preprint (which was not certified by peer review) is the author/funder, who has granted bioRxiv a license to display the preprint in perpetuity. It is made available under aCC-BY-NC 4.0 International license.

691 Histograms of the fraction of confined Lck^{K273R}-PAmCherry molecules obtained for 12
692 stimulated (blue) and 14 resting (orange) Jurkat cells and histograms of the fraction of
693 confined Lck$^{K273R, Y505F}$-PAmCherry obtained for 8 stimulated (yellow) and 8 resting (purple)
694 Jurkat cells. Box plot shows the median. Notch 95% confidence interval, box edges first and
695 third quartile, lines Tukey's fences, , **** $p \leq 0.00001$, n.s. $p > 0.01$.
696

bioRxiv preprint doi: https://doi.org/10.1101/446732; this version posted October 18, 2018. The copyright holder for this preprint (which was not certified by peer review) is the author/funder, who has granted bioRxiv a license to display the preprint in perpetuity. It is made available under aCC-BY-NC 4.0 International license.

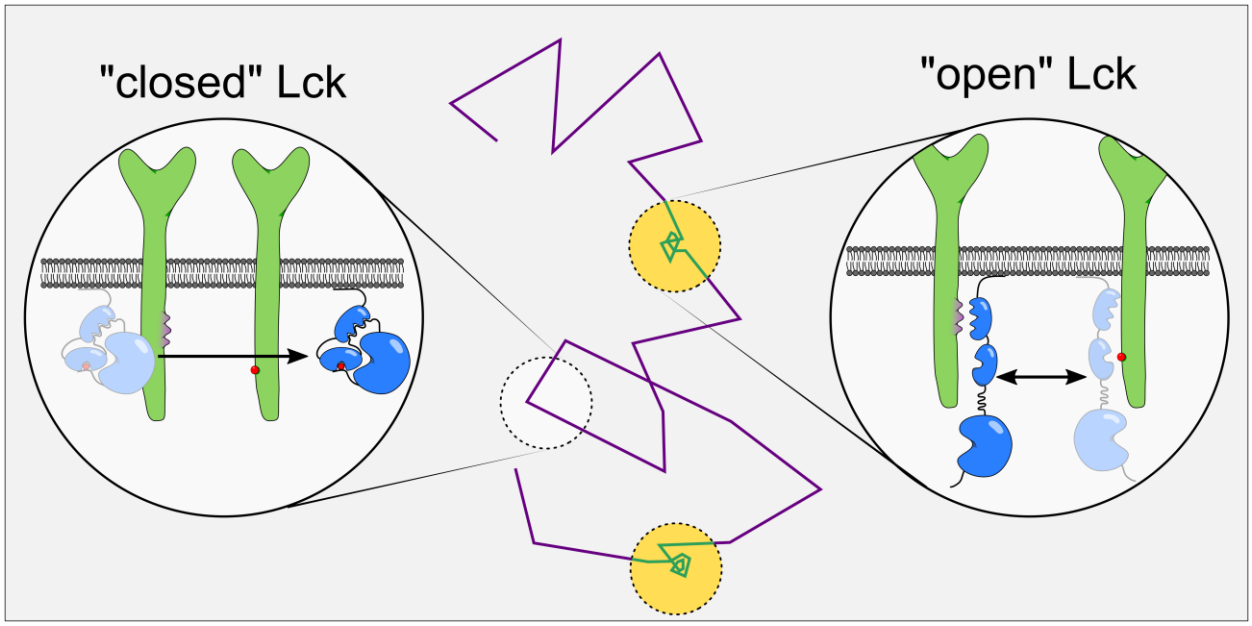

Fig. 7 Two-stage diffusion model of Lck that combines an efficient search strategy with a high phosphorylation rates of substrates. Lck (illustrated in blue) exists in two main conformations: a closed conformation characterized by low catalytic activity and mediated by intramolecular interactions; and an open conformation characterized by high catalytic activity and free SH2 and SH3 domains. Our data propose that the closed conformation diffuses unimpeded (purple line), whereas the open conformation interacts with other membrane proteins (illustrated in green) via SH2 and SH3 domain mediated interactions and becomes confined (yellow circles) through rapid rebinding (teal line). Free diffusion allows Lck to scan large membrane areas while confinement in the open conformation enables high substrate phosphorylation rates.